PAPER • OPEN ACCESS

Unveiling the origin of the basal-plane antiferromagnetism in the spin–orbit Mott insulator Ba_2IrO_4: a density functional and model Hamiltonian study

To cite this article: Y S Hou *et al* 2016 *New J. Phys.* **18** 043007

New Journal of Physics
The open access journal at the forefront of physics

Deutsche Physikalische Gesellschaft DPG
IOP Institute of Physics

Published in partnership with: Deutsche Physikalische Gesellschaft and the Institute of Physics

OPEN ACCESS

RECEIVED
10 December 2015

REVISED
25 February 2016

ACCEPTED FOR PUBLICATION
7 March 2016

PUBLISHED
7 April 2016

PAPER

Unveiling the origin of the basal-plane antiferromagnetism in the spin–orbit Mott insulator Ba_2IrO_4: a density functional and model Hamiltonian study

Y S Hou, H J Xiang and X G Gong

Key Laboratory of Computational Physical Sciences (Ministry of Education), State Key Laboratory of Surface Physics, Collaborative Innovation Center of Advanced Microstructures, and Department of Physics, Fudan University, Shanghai 200433, People's Republic of China

E-mail: hxiang@fudan.edu.cn **and** xggong@fudan.edu.cn

Keywords: density-functional theory, antiferromagnetic materials, exchange interactions, Heisenberg–Kitaev model

Abstract

Based on the density functional theory and model Hamiltonian, we studied the basal-plane antiferromagnetism in the spin–orbit Mott insulator Ba_2IrO_4. By comparing the magnetic properties of the bulk Ba_2IrO_4 with those of the single-layer Ba_2IrO_4, we demonstrate unambiguously that the basal-plane antiferromagnetism is caused by the intralayer magnetic interactions rather than by the previously proposed interlayer ones. Aiming at revealing the origin of the basal-plane antiferromagnetism, we add the single ion anisotropy and pseudo-quadrupole interactions into the general bilinear pseudo-spin Hamiltonian. The obtained magnetic interaction parameters indicate that the single ion anisotropy and pseudo-quadrupole interactions are unexpectedly strong. Systematical Monte Carlo simulations demonstrate that the basal-plane antiferromagnetism is caused by isotropic Heisenberg, bond-dependent Kitaev and pseudo-quadrupole interactions. On the basis of this study the single ion anisotropy and pseudo-quadrupole interactions could play a role in explaining magnetic interactions in other iridates.

1. Introduction

Recently, iridium oxides have been extensively studied both experimentally and theoretically because many exotic and emerging phenomena are proposed to be realized in such iridium oxides [1, 2]. For example, quantum spin Hall effect has been predicted in Na_2IrO_3 [3, 4]. Topological Mott insulator [5, 6], Weyl semimetal and axion insulator [7] are theoretically shown to exist in the pyrochlore iridium oxides. Most excitingly, iridium oxides with the honeycomb lattice are greatly expected to realize the long-sought Kitaev model, which has an exactly solvable quantum spin liquid ground state [8–11]. Furthermore, some theoretical and experimental studies suggested that the prototypical iridium oxide Sr_2IrO_4 (SIO) could display an unconventional high-T_C superconductivity [12–15]. However, the appreciable ferromagnetic (FM) moment arising from the rotationally distorted IrO_6 octahedron in SIO may easily break the spin-singlet Cooper pairs [16, 17]. Therefore other iridium oxides need to be explored. It is found that the square-lattice antiferromagnet Ba_2IrO_4 (BIO) crystallizes in the space group I4/mmm [18] and is a closer analogue to the layered La_2CuO_4 than SIO [19]. It is therefore expected that BIO is suitable for realizing the high-T_C superconductivity.

However, there remains a fundamental and important issue regarding the basal-plane antiferromagnetism in BIO to be clarified. Experimentally, it is found that the magnetic moments of Ir^{4+} ions are antiferromagnetically coupled and point along the [110] direction [18–21]. Katukuri *et al* theoretically investigated [22] how the [110]-pointing antiferromagnetism is established. Based on the general bilinear pseudo-spin Hamiltonian, they proposed that the experimentally observed basal-plane antiferromagnetism could be accounted for by including the additional interlayer magnetic interactions and the associated order-by-disorder quantum-mechanical effects [22]. However, the interlayer magnetic interactions in BIO may be too

weak to play a dominant role in establishing the experimentally observed basal-plane antiferromagnetism, because the shortest distance between the interlayer Ir^{4+} ions is about 7.3 Å [18] and the interlayer Ir^{4+} ions are separated by two BaO layers. Therefore, it will be of great importance to reinvestigate the origin of the experimentally observed basal-plane antiferromagnetism in BIO.

In this paper, we put forward a new mechanism to explain the experimentally observed basal-plane antiferromagnetism in BIO, based on the density functional theory (DFT), model Hamiltonian, and Monte Carlo (MC) simulations. Firstly, the comparison of the magnetic properties, especially the basal-plane magneto-crystalline anisotropy energy (MAE), between the bulk and single-layer BIO clearly demonstrates that the experimentally observed basal-plane antiferromagnetism is caused by the intralyer magnetic interactions rather than by the previously proposed interlayer ones [22]. Next, it is proved that the calculated basal-plane MAE cannot be explained by the general bilinear pseudo-spin Hamiltonian. To bring to light the origin of the experimentally observed basal-plane antiferromagnetism, we add the single ion anisotropy (SIA) and pseudo-quadrupole interaction into the general bilinear pseudo-spin Hamiltonian. By computing the magnetic interaction parameters in the model Hamiltonian, we find that the SIA and pseudo-quadrupole interaction are unexpectedly strong in BIO. Based on the systematical MC simulations, we demonstrate that the experimentally observed basal-plane antiferromagnetism can be explained by the isotropic Heisenberg, bond-dependent Kitaev and pseudo-quadrupole interactions. On the basis of this study the SIA and pseudo-quadrupole interactions could play a role in explaining magnetic interactions in other iridates.

2. Computational methods

Our first-principles calculations are based on the DFT and performed within the generalized gradient approximation according to the Perdew–Burke–Ernzerhof parameterization as implemented in Vienna *Ab initio* Simulation Package [23]. In this work, we use the projector-augmented wave method [24] with an energy cutoff of 450 eV and a gamma-centered $7 \times 7 \times 3$ k-point mesh grid. Besides, the experimental measured structure [18] and the $\sqrt{2} \times \sqrt{2} \times 1$ supercell containing 4 Ir^{4+} ions to accommodate the antiferromagnetic (AFM) state are adopted. To describe the electron correlation associated with the 5d electron of Ir^{4+} ions, we use the rotationally invariant DFT + U scheme introduced by Liechtenstein *et al* [25]. The on-site Coulomb energy $U = 2.5$ eV and the Hund coupling $J_H = 0.5$ eV [2, 26, 27] are applied to the Ir 5d electrons. Because Ir is a kind of heavy element and its relativistic spin-orbit coupling (SOC) ($\lambda = 0.45$ eV) [28, 29] is rather strong, SOC is taken into consideration in calculating the initial magnetic ground state, basal-plane MAE and the magnetic interactions parameters. The efficient exchange MC method is employed for finding the magnetic ground state [30, 31].

3. Result and discussion

In this section, we first demonstrate that the basal-plane antiferromagnetism in BIO is caused by the intralayer magnetic interactions instead of the previously proposed interlayer ones [22]. We then prove the basal-plane MAE of BIO can be phenomenologically accounted for by adding the SIA and pseudo-quadrupole interactions into the general bilinear pseudo-spin Hamiltonian. Finally, we demonstrate the experimentally observed basal-plane antiferromagnetism of BIO can be explained by the isotropic Heisenberg, bond-dependent Kitaev and pseudo-quadrupole interactions.

3.1. DFT study on the basal-plane antiferromagnetism in BIO

Bulk BIO is a spin–orbit Mott insulator and has the quasi-two-dimensional lattice structure and tetragonal symmetry [18]. It consists of single-layer BIO perovskites and these single-layer BIO perovskites stack along the z-axis, i.e., the [001] direction (see figure 1(a)). There are two single-layer BIO perovskites in the unit cell of bulk BIO. In the tetragonal xy-plane, Ir^{4+} ions are located at the center of the corner-sharing oxygen octahedrons which have a 7% tetragonal distortion along the z-axis [18]. The IrO_2 square-lattice planes are separated by two successive BaO layers and the Ir^{4+} ions in the neighboring IrO_2 square-lattice planes are spatially separated as far as about 7.3 Å [18] (see figure 1(a)). Recent experiments show that the crystal field splitting associated with the tetragonal distortion of the IrO_6 octahedron is small so that BIO is a close realization of the spin–orbit Mott insulator [32].

Based on the DFT + U + SOC calculation, we first confirm the magnetic ground state of the bulk BIO to be the AFM state with the magnetic moment of Ir^{4+} ions pointing along the [110] direction, which is in consistent with the experimental observation [18]. Here we take into account three representative AFM states: the AFM state with the magnetic moment of the Ir^{4+} ions pointing along the [001] direction (denoted as AFM-001), along the [100] direction (denoted as AFM-100) and along the [110] direction (denoted as AFM-110) (see figure 1(b)).

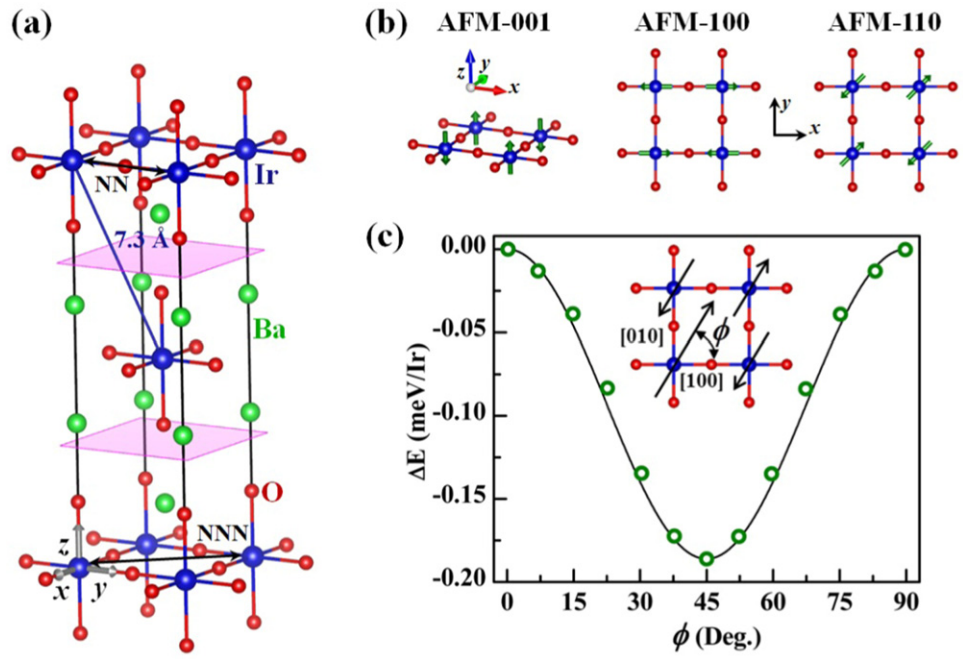

Figure 1. (a) Lattice structure of the bulk Ba_2IrO_4. Green, blue and red spheres represent Ba, Ir and O atoms, respectively. The NN and NNN Ir–Ir pairs are connected by black double-arrow solid lines. The shortest distance (7.3 Å) between the two Ir^{4+} ions in the neighboring IrO_2 square-lattice planes is shown by the solid blue line. The structure unit, i.e., the single-layer Ba_2IrO_4 perovskite, is sandwiched by the two pink rectangles. The global *xyz* coordinate system is shown by the gray arrows. Note that the [100], [010] and [001] directions correspond to *x*, *y*, *z*-axes, respectively. (b) The magnetic structures of the representative AFM-001, AFM-100 and AFM-110 states. The magnetic moments of the Ir^{4+} ions are represented by green arrows. (c) The dependence of the total energy of the basal-plane AFM state on the polar angle ϕ. The open green circles show the total energy obtained by the DFT + *U* + SOC calculations. The solid line shows the fitted total energy based on the MAE defined by equation (2). The inset shows the definition of the polar angle ϕ of the basal-plane AFM state with respect to the [100] direction.

Although the total energy of the AFM-100 state is lower by 1.7 meV/Ir than that of the AFM-001 state, it is slightly higher by 0.19 meV/Ir than that of the AFM-110 state. It is worth of noting that if the initial state is the FM state, it cannot be stabilized and the resulting state is the paramagnetic state and has a higher total energy than the AFM-001, AFM-100 and AFM-110 states.

Then we investigate in details the basal-plane MAE of the bulk BIO and find that the basal-plane MAE can be fitted to a formula which includes the four-order contribution. Since the AFM state cannot be accommodated by the unit cell of the bulk BIO which has only one Ir^{4+} ion per IrO_2 square-lattice plane, we use the $\sqrt{2} \times \sqrt{2} \times 1$ supercell containing two Ir^{4+} ions per IrO_2 square-lattice plane. To obtain the basal-plane MAE, we constrain the magnetic moments of the antiferromagnetically coupled Ir^{4+} ions in the tetragonal *xy*-plane and rotate them by an angle ϕ with respect to the [100] direction (see the inset of figure 1(c)). Figure 1(c) shows the dependence of the DFT + *U* + SOC calculated total energy on the rotated angle ϕ. As is expected, the minimum of the total energy occurs at $\phi = 45°$, i.e., at the [110] direction. Because of the tetragonal symmetry, MAE can be approximated in the form of [33]

$$E(\theta, \phi) = K_1 \sin^2\theta + K_2 \sin^4\theta + K_3 \sin^4\theta \sin^2\phi \cos^2\phi + E_0'. \quad (1)$$

In equation (1), θ and ϕ are the azimuthal and polar angles with respect to the [001] direction (*z*-axis) and [100] direction (*x*-axis), respectively. Because the magnetic moments of the Ir^{4+} ions of the considered AFM states lie in the tetragonal *xy*-plane, θ is equal to $\pi/2$ and the first and second terms in equation (1) become constant. Thus the MAE in equation (1) reduces to

$$E(\theta = \pi/2, \phi) = K_3 \sin^2\phi \cos^2\phi + E_0. \quad (2)$$

Note that the constant K_1 and K_2 in equation (1) are absorbed into the constant E_0. Based on equation (2), the fitted MAE parameter K_3 is 2.8×10^6 erg cm^{-3}, one order of magnitude larger than that of the body-center cubic iron [34].

To make clear the effect of the interlayer magnetic interactions on the basal-plane antiferromagnetism, we investigate the magnetic properties of the single-layer BIO. The lattice structure of the single-layer BIO is shown in the figure 2(a). It consists of one of the single-layer BIO perovskite and vacuum layers. The thickness of the vacuum region is 9.02 A. Because the Ir^{4+} ions in the IrO_2 square-lattice planes are isolated by the thick enough vacuum layers, the interlayer magnetic interactions existing in the bulk BIO vanish in the single-layer BIO. Note

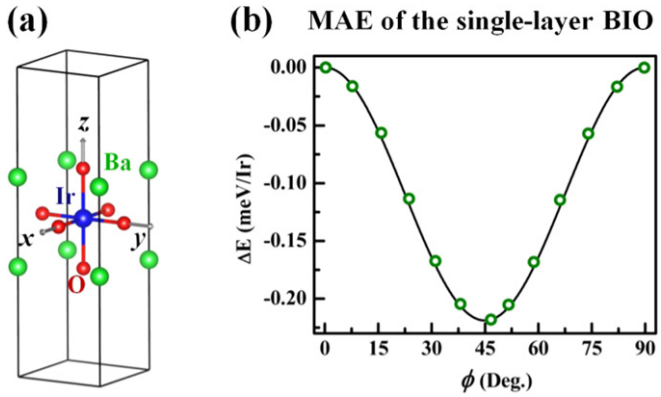

Figure 2. (a) Lattice structure of the single-layer Ba_2IrO_4. Ba, Ir and O atoms are represented by the green, blue and red spheres, respectively. The global *xyz* coordinate system is shown by the gray arrows. (b) The dependence of the total energy of the basal-plane AFM state on the polar angle ϕ. The open green circles show the total energy obtained by the DFT + U + SOC calculations. The solid line shows the fitted total energy based on the MAE defined by equation (2).

that although the single-layer BIO (space group P4/mmm) has a slightly lower symmetry than the bulk BIO (space group I4/mmm), it preserves the vital tetragonal symmetry. Surprisingly, we find the interlayer magnetic interactions have no significant effect on the basal-plane antiferromagnetism, because the single-layer BIO almost reproduces the magnetic properties of the bulk BIO. First of all, the magnetic ground state of the single-layer BIO is the AFM-110 state. Secondly, the AFM-100 state has the higher total energy than the AFM-110 state but has the lower total energy than the AFM-001 state. Most importantly, the single-layer BIO has almost the same basal-plane MAE as the bulk BIO. Using the same method applied to the calculation of the basal-plane MAE of the bulk BIO, we obtain the basal-plane MAE of the single-layer BIO and show it in the figure 2(b). By comparing the figures 1(c) and 2(b), one can come to a conclusion that the profile of the basal-plane MAE of the single-layer BIO is almost the same as that of the bulk BIO. Based on equation (2), the fitted MAE constant K_3 of the single-layer BIO is 2.9 $\times$ 10^6 erg cm^{-3}, very close to that of the bulk BIO. Therefore, it is clearly demonstrated that the experimentally observed basal-plane antiferromagnetism is caused by the intralayer magnetic interactions instead of the interlayer ones. It also implies that the interlayer magnetic interactions are negligible compared with the intralayer ones, which will be discussed below (see table 1). Note that our result is distinctly different from the previous one which argued that interlayer magnetic interactions could have significant effect on the experimentally observed basal-plane antiferromagnetism [22].

3.2. Model Hamiltonian study on the basal-plane antiferromagnetism in BIO

Here we first recall the Hamiltonian employed by the previous studies on the iridium oxides [8, 22, 35, 36]. The Ir^{4+} ions yields an effective isospin Kramers-doublet ground states due to the strong octahedral crystal field and SOC [8, 20, 32]. The Kramers-doublet ground states are the pseudo-spin states $|\tilde{\uparrow}\rangle$ and $|\tilde{\downarrow}\rangle$ (denoted as $\overline{\boldsymbol{S}}$ to be distinguished from the usual spin $\boldsymbol{S}$) which are in the form of [8]:

$$|\tilde{\uparrow}\rangle = \sin\alpha\,|xy,\uparrow\rangle + \frac{\cos\alpha}{\sqrt{2}}(\mathrm{i}\,|xz,\downarrow\rangle + |yz,\downarrow\rangle), \tag{3.1}$$

$$|\tilde{\downarrow}\rangle = \sin\alpha\,|xy,\downarrow\rangle + \frac{\cos\alpha}{\sqrt{2}}(\mathrm{i}\,|xz,\uparrow\rangle - |yz,\uparrow\rangle). \tag{3.2}$$

In equations (3.1) and (3.2), the angle α parameterizes the relative strength of the tetragonal crystal-field splitting and $\tan(2\alpha) = 2\sqrt{2}\,\lambda/(\lambda - \Delta)$ (Δ and λ are the tetragonal crystal-field splitting and SOC parameter, respectively). For a pair of pseudo-spins $\overline{\boldsymbol{S}}_i$ and $\overline{\boldsymbol{S}}_j$, the general bilinear pseudo-spin Hamiltonian can be cast in the form of [8, 22, 35, 36]

$$H_{ij} = J_{ij}^{\mathrm{H}}\,\overline{\boldsymbol{S}}_i \cdot \overline{\boldsymbol{S}}_j + J_{ij}^{\mathrm{K}}\,\overline{\boldsymbol{S}}_i^{\gamma}\,\overline{\boldsymbol{S}}_j^{\gamma} + D_{ij} \cdot (\overline{\boldsymbol{S}}_i \times \overline{\boldsymbol{S}}_j) + J_{ij}^{\mathrm{DP}}(\overline{\boldsymbol{S}}_i \cdot r_{ij})(r_{ij} \cdot \overline{\boldsymbol{S}}_j). \tag{4}$$

In equation (4), $\boldsymbol{r}_{ij}$ is the unit vector along the *ij* bond and γ is anyone of the *x*, *y* and *z*. The first term is the isotropic Heisenberg interaction. The second term is the celebrated bond-dependent Kitaev interaction (see the [8] for the details). The tetragonal symmetry of BIO requires that only the $J_{ij}^{\mathrm{K}}\,\overline{S}_i^z\,\overline{S}_j^z$ term may not vanish [8], when the *z*-axis of the global coordinate system is set to be perpendicular to the IrO_2 square-lattice plane (see the global coordinate system plotted in the figure 1(a)). The third term is the Dzyaloshinskii–Moriya (DM) interactions but it vanishes in BIO. The last term is the pseudo-dipolar interaction. For convenience, hereafter, the magnitude of the pseudo-spin is absorbed into the magnetic interactions parameters J_{ij}^{H}, J_{ij}^{K} and J_{ij}^{DP}, so the pseudo-spin vectors $\overline{\boldsymbol{S}}_i$ and $\overline{\boldsymbol{S}}_j$ become a unit vector.

We show here that the general pseudo-spin Hamiltonian defined by equation (4) cannot explain the calculated basal-plane MAE of the bulk BIO. Because the interlayer magnetic interactions are demonstrated to be negligible compared to the intralayer ones, they are left out of consideration here. We consider an arbitrary AFM state with the magnetic moments of the Ir^{4+} ions pointing along the direction (θ, ϕ) in the $\sqrt{2} \times \sqrt{2} \times 1$ supercell and denote such state as AFM(θ, ϕ). Firstly, the isotropic Heisenberg interaction has the SO(3) symmetry so it makes no contribution to the MAE. Secondly, the contribution from the nearest neighboring (NN) and next nearest neighboring (NNN) Kitaev interactions to the MAE is (see appendix A)

$$E^{\mathrm{K}}(J^{\mathrm{K}}, \theta, \phi) = -8J_1^{\mathrm{K}} \cos^2\theta + 8J_2^{\mathrm{K}} \cos^2\theta. \tag{5}$$

In equation (5), J_1^{K} and J_2^{K} are the NN and NNN bond-dependent Kitaev interactions parameters, respectively. Thirdly, the contributions from the NN and NNN pseudo-dipole interactions to the MAE are (see the appendix A)

$$E^{DP}(J^{DP}, \theta, \phi) = -4J_1^{DP} \sin^2\theta + 4J_2^{DP} \sin^2\theta. \tag{6}$$

In equation (6), J_1^{DP} and J_2^{DP} are the NN and NNN pseudo-dipole interactions parameters, respectively. Therefore, the contribution from the NN and NNN bond-dependent Kitaev and pseudo-dipole interactions to the MAE of an arbitrary AFM(θ, ϕ) state is only dependent on the azimuthal angle θ and independent on the polar angle ϕ. We can further demonstrate that even if the negligible bond-dependent Kitaev and pseudo-dipole interactions of the Ir–Ir pairs farther than the NNN Ir–Ir one are taken into consideration, their contribution to the MAE still only depends on the azimuthal angle θ (see the equation (A.3) in the appendix A). In summary, one can conclude based on the general pseudo-spin Hamiltonian defined by equation (4) that the basal-plane AFM state ($\theta = \pi/2$) is isotropic, which contradicts with the experimentally observed [110]-pointing AFM state [20].

In this work, we add the SIA and pseudo-quadrupole interaction into the general pseudo-spin Hamiltonian defined by equation (4). Although it is commonly believed that magnetic systems made up of transition-metal ions with one unpaired electron have no magnetic anisotropy arising from SOC [37], our recent work showed that most such transition-metal ions did have the SIA [38, 39]. Because the pseudo-spin $\overline{\boldsymbol{S}}$ state is an analogy to the spin state in the transition-metal ion with one unpaired electron, it is natural to generalize that the pseudo-spin $\overline{\boldsymbol{S}}$ does have the SIA which is in the form of $A^{\mathrm{SIA}}(\overline{S}^z)^2$. Note that the non-zero SIA has been pointed out to be present in Na_2IrO_3 [40] and SIO [41] (See the theoretical and numerical demonstration and discussion of the SIA of the pseudo-spin state in the appendix B.) For the same reason, we further generalize that the quadrupole-quadrupole coupling proposed by Van Vleck [42] can also exist in the pseudo-spin $\overline{\boldsymbol{S}}$ systems:

$$H_{ij}^{\mathrm{QP}} = J_{ij}^{\mathrm{QP}} (\overline{\boldsymbol{S}}_i \cdot \boldsymbol{r}_{ij})^2 (\boldsymbol{r}_{ij} \cdot \overline{\boldsymbol{S}}_j)^2. \tag{7}$$

In equation (7), J_{ij}^{QP} and $\boldsymbol{r}_{ij}$ are the pseudo-quadrupole interaction parameter and the unit vector along the ij bond, respectively.

Now let us demonstrate the calculated basal-plane MAE can be well accounted for on the basis of the above model Hamiltonian. For an arbitrary AFM(θ, ϕ) state in the $\sqrt{2} \times \sqrt{2} \times 1$ supercell, the contributions from the NN and NNN pseudo-quadrupole interactions to the MAE is (see the appendix A)

$$E^{\mathrm{QP}}(J^{\mathrm{QP}}, \theta, \phi) = \sin^4\theta\,[4J_1^{\mathrm{QP}}(1 - 2\sin^2\phi\cos^2\phi) + 2J_2^{\mathrm{QP}}(1 + 4\sin^2\phi\cos^2\phi)]. \tag{8}$$

In equation (8), J_1^{QP} and J_2^{QP} are the NN and NNN pseudo-quadrupole interaction parameters, respectively. Since the pseudo-quadrupole interaction is a kind of short-range interaction, it is reasonable that only the NN and NNN pseudo-quadrupole interactions are taken into account. Taking into consideration the isotropic Heisenberg, bond-dependent Kitaev, pseudo-dipole and pseudo-quadrupole interactions of the NN and NNN Ir–Ir pairs and the SIA, we obtain their contribution to the MAE of an arbitrary AFM(θ, ϕ) state as follows:

$$E(\theta, \phi) = K_1 \sin^2\theta + K_2 \sin^4\theta + K_3 \sin^4\theta \sin^2\phi \cos^2\phi + E_0. \tag{9}$$

The coefficients in equation (9) are

$$K_1 = 8J_1^{\mathrm{K}} - 8J_2^{\mathrm{K}} - 4J_1^{\mathrm{DP}} + 4J_2^{\mathrm{DP}} - 4A^{\mathrm{SIA}}, \tag{9.1}$$

$$K_2 = 4J_1^{\mathrm{QP}} + 2J_2^{\mathrm{QP}}, \tag{9.2}$$

$$K_3 = -8J_1^{\mathrm{QP}} + 8J_2^{\mathrm{QP}}. \tag{9.3}$$

When the magnetic moments of the Ir^{4+} ions lie on the tetragonal xy-plane, i.e., $\theta = \pi/2$, equation (9) reduces to $K_3 \sin^2\phi \cos^2\phi + C$, which is the same as equation (2) and indicates that the basal-plane AFM state is anisotropic instead of isotropic. Furthermore, if the coefficient K_3 is negative, the energy of the basal-plane AFM state reaches its minimum when the magnetic moments of the Ir^{4+} ions point along the [110] direction. So the experimentally observed basal-plane antiferromagnetism can be phenomenologically explained by adding the pseudo-quadrupole interactions and the SIA into the generalized pseudo-spin Hamiltonian defined by equation (4).

Table 1. The considered magnetic interaction and SIA parameters are obtained by means of the DFT + U + SOC calculations and given in units of meV. The calculated SIA parameter is $A^{\mathrm{SIA}} = -6.46$ meV. As for the NNNN and interlayer Ir–Ir pairs, only the isotropic Heisenberg interactions are calculated.

Ir–Ir pairs	J^{H}	J^{K}	J^{DP}	J^{QP}
NN	36.17	−0.75	−0.14	1.61
NNN	−11.46	4.58	0.15	1.23
NNNN	1.92	—	—	—
Interlayer	−0.14	—	—	—

Therefore the model Hamiltonian which well describes the magnetic behavior of BIO should be in the form of

$$\begin{aligned} H = & \sum_{\langle i,j\rangle \in xy} [J_{ij}^{\mathrm{H}} \overline{\boldsymbol{S}}_i \cdot \overline{\boldsymbol{S}}_j + J_{ij}^{\mathrm{K}} \overline{S}_i^z \overline{S}_j^z + J_{ij}^{\mathrm{DP}} (\overline{\boldsymbol{S}}_i \cdot \boldsymbol{r}_{ij})(\boldsymbol{r}_{ij} \cdot \overline{\boldsymbol{S}}_j) + J_{ij}^{\mathrm{QP}} (\overline{\boldsymbol{S}}_i \cdot \boldsymbol{r}_{ij})^2 (\boldsymbol{r}_{ij} \cdot \overline{\boldsymbol{S}}_j)^2] \\ & + \sum_{\langle\langle i,j\rangle\rangle \in xy} [J_{ij}^{\mathrm{H}} \overline{\boldsymbol{S}}_i \cdot \overline{\boldsymbol{S}}_j + J_{ij}^{\mathrm{K}} \overline{S}_i^z \overline{S}_j^z + J_{ij}^{\mathrm{DP}} (\overline{\boldsymbol{S}}_i \cdot \boldsymbol{r}_{ij})(\boldsymbol{r}_{ij} \cdot \overline{\boldsymbol{S}}_j) + J_{ij}^{\mathrm{QP}} (\overline{\boldsymbol{S}}_i \cdot \boldsymbol{r}_{ij})^2 (\boldsymbol{r}_{ij} \cdot \overline{\boldsymbol{S}}_j)^2] \\ & + \sum_i A_i^{\mathrm{SIA}} (\overline{S}_i^z)^2. \end{aligned} \tag{10}$$

In equation (10), the first and second terms describe the magnetic interactions of the NN and NNN Ir–Ir pairs in the tetragonal xy-plane, respectively. Note that the isotropic Heisenberg, bond-dependent Kitaev, pseudo-dipole and pseudo-quadrupole interactions are all taken into consideration for the NN and NNN Ir–Ir pairs in the tetragonal xy-plane. The last term is the SIA generalized in our present work. Because the distances of the third nearest neighboring (NNNN) Ir–Ir pairs in the tetragonal xy-plane and the interlayer Ir–Ir pairs are 8.1 Å and 7.3 Å, respectively, their Heisenberg interactions should be rather weak. This is confirmed by our calculations (see table 1). Compared to the isotropic Heisenberg interaction, their bond-dependent Kitaev, pseudo-dipole and pseudo-quadrupole interactions are much weaker and thereby left out of consideration hereafter.

The considered magnetic interactions and SIA parameters are obtained based on the DFT + U + SOC calculations (see appendix C for the detailed calculation) and listed in the table 1. It is shown that the dominant magnetic interactions are the NN AFM and NNN FM Heisenberg interactions. So it is undoubted that the magnetic ground state should be AFM. Note that our calculated NN AFM Heisenberg interaction is well consistent with the previously calculated one [22, 43]. Besides, there are several important points being worth of noting. Firstly, it is beyond expectation that the NN bond-dependent Kitaev interaction has a much smaller magnitude than the NNN bond-dependent Kitaev interaction. Actually, this is reasonable and understandable. The NN bond-dependent Kitaev interaction is realized through the 180° Ir–O–Ir bond so it should be rather weak [8], as the calculated one. However, it has been shown that there exists a large Kitaev interaction in slightly distorted 90° Ir–O–Ir bond of Na_2IrO_3 [8, 44]. Therefore it is expected that the four distorted Ir–O–Ir bonds (116.5°) facilitate and result in the unexpectedly large NNN Kitaev interaction (see the inset of figure 3(a)). Secondly, the pseudo-quadrupole interaction and the SIA are both strong, which is a manifestation of the strong SOC in iridium oxides. Finally, the NNNN and interlayer Heisenberg interactions are very weak, as expected. Note that the former and the latter are smaller by one order and by two orders than the NN Heisenberg interaction, respectively. An important reason for such weak interlayer Heisenberg interaction is that two BaO layers embed into the neighboring IrO_2 planes prevent the electron from hopping between the interlayer Ir^{4+} ions. Because the NNNN and interlayer Heisenberg interactions are much weaker than the NN and NNN Heisenberg interactions, they will be left out of consideration in the below discussion.

In order to make clear how the bond-dependent Kitaev, pseudo-dipole and pseudo-quadrupole interactions and the SIA affect the antiferromagnetism of BIO, we investigate the dependence of the energy differences $\Delta E1 = E$(AFM-001)–E(AFM-110) and $\Delta E2 = E$(AFM-100)–E(AFM-110) on them. Based on equation (9), the energy difference $\Delta E1$ and $\Delta E2$ are calculated by linearly increasing the NN and NNN bond-dependent Kitaev interaction parameters from the vanishing ones ($J^{\mathrm{K}}/J_0^{\mathrm{K}} = 0$) to the DFT + U + SOC calculated ones ($J^{\mathrm{K}}/J_0^{\mathrm{K}} = 1$) while keeping other magnetic interaction parameters unchanged. The similar method is applied to calculate the dependence of $\Delta E1$ and $\Delta E2$ on the pseudo-dipole and pseudo-quadrupole interactions and the SIA parameters. Figure 3(a) shows the energy difference $\Delta E1$ gets larger and larger as the bond-dependent Kitaev interaction becomes stronger and stronger. This indicates the bond-dependent Kitaev interaction does not favor the magnetic moments of the Ir^{4+} ions to point along the z-axis. In the figures 3(b)–(d), the energy difference $\Delta E1$ gets smaller and smaller as the corresponding pseudo-dipole, pseudo-quadrupole interactions and the SIA become stronger and stronger. This indicates that the pseudo-dipole, pseudo-quadrupole

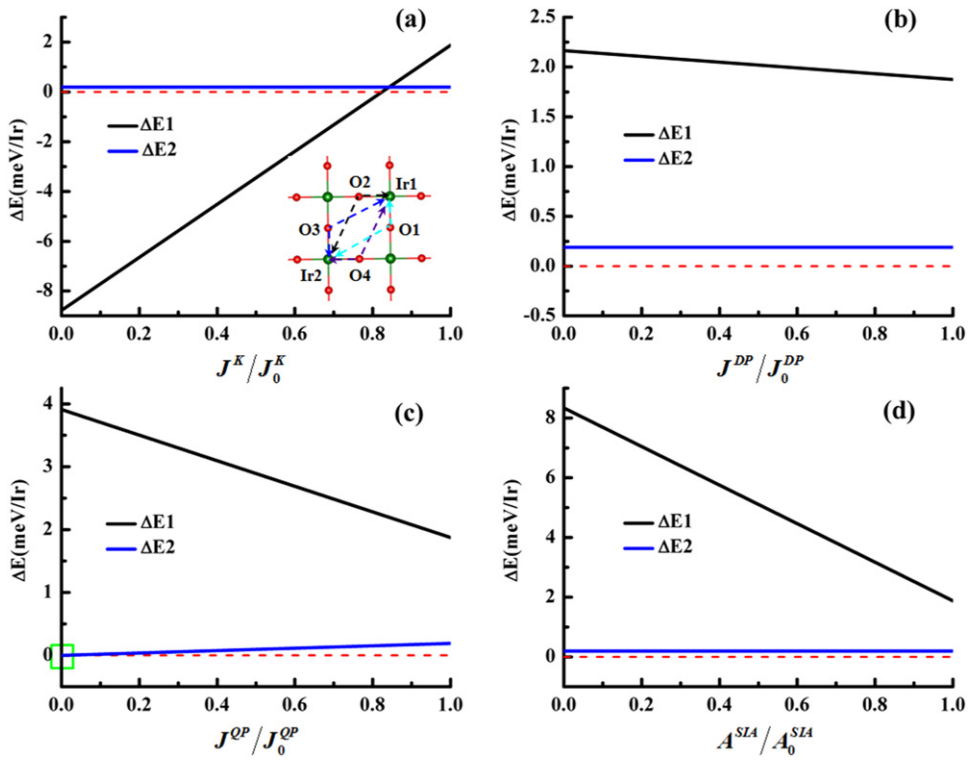

Figure 3. The dependence of the energy differences $\Delta E1 = E$(AFM-001)–E(AFM-110) (black line) and $\Delta E2 = E$(AFM-100)–E(AFM-110) (blue line) on the bond-dependent Kitaev interaction (a), pseudo-dipole interaction (b), pseudo-quadrupole interaction (c) and SIA (d). J_0^{K}, J_0^{DP}, J_0^{QP} and A_0^{SIA} are the DFT + U + SOC calculated bond-dependent Kitaev, pseudo-dipole and pseudo-quadrupole interactions and the SIA parameters, respectively. The red lines in (a), (b), (c) and (d) are for eye guidance. In (a), the inset shows the four 116.5° Ir–O–Ir bonds of the specified NNN Ir1–Ir2 pair. The four Ir–O–Ir bonds are depicted by the dashed black, blue, purple and cyan lines. In (c), the point ($J^{\mathrm{QP}}/J_0^{\mathrm{QP}} = 0$, $\Delta E2 = 0$) is highlighted by the green square.

interactions, and the SIA favor the magnetic moments of the Ir^{4+} ions to point along the z-axis. Because the energy difference $\Delta E2$ plotted in the figures 3(a), (b) and (d) has nothing to do with the corresponding bond-dependent Kitaev, pseudo-dipole interactions and SIA, one can conclude that they are not relevant to the fact that the magnetic moments of the Ir^{4+} ions point along the [110]-direction. However, the energy difference $\Delta E2$ plotted in the figure 3(c) indicates that the AFM-110 and AFM-100 states are degenerate if the pseudo-quadrupole interaction is vanished and this degeneracy can be broken by the non-vanished pseudo-quadrupole interaction. Furthermore, the energy difference $\Delta E2$ gets larger and larger as the pseudo-quadrupole interaction becomes stronger and stronger. So the pseudo-quadrupole interaction drives the magnetic moments of the Ir^{4+} ions to point along the [110]-direction.

Finally, we show that the experimentally observed AFM-110 state is caused by the isotropic Heisenberg, bond-dependent Kitaev and pseudo-quadrupole interactions, based on the systematical MC simulations (see table 2). Because the isotropic Heisenberg interaction is the dominant magnetic interaction, it is always included in the MC simulations. However, the bond-dependent Kitaev, pseudo-dipole and pseudo-quadrupole interactions and the SIA are optionally included in the MC simulations. By comparing the Case 1 and 2 listed in the table 2, one can obtain that, for the antiferromagnetically coupled Ir^{4+} ions, the bond-dependent Kitaev interaction makes their magnetic moments lie at the tetragonal xy-plane with the continuous degeneracy. However, Case 7 clearly shows the pseudo-quadrupole interaction can break the above-mentioned continuous degeneracy and the resulting magnetic structure is just the experimentally observed AFM-110 state. By carefully investigating the table 2, we can obtain that: (1) the magnetic ground state is the basal-plane AFM state with the magnetic moments of the Ir^{4+} ions lying in the tetragonal xy-plane as long as the Heisenberg and Kitaev interactions are taken into account; (2) the magnetic ground state is the experimentally observed AFM-110 state as long as the isotropic Heisenberg, bond-dependent Kitaev and pseudo-quadrupole interactions are taken into account; (3) although the pseudo-dipole, pseudo-quadrupole interactions, and the SIA favor the magnetic moments of the Ir^{4+} ions to point along the z-axis (see the Case 3, 4 and 5 in the table 2), they cannot destroy the basal-plane AFM state established by the isotropic Heisenberg and bond-dependent Kitaev interactions. To sum up, it is clearly shown that the experimentally observed AFM-110 state can be explained by the isotropic Heisenberg, bond-dependent Kitaev and pseudo-quadrupole interactions.

Table 2. Magnetic ground states obtained from systematical MC simulations in which different magnetic interactions are included. Plus sign (+) means the corresponding magnetic interaction is included in the MC simulations while the minus sign (−) means the corresponding magnetic interaction is not included in the MC simulations. The two-fold degeneracy of the AFM-001 state results from the time reversal invariance and the eight-fold degeneracy of the AFM-110 state results from the time reversal invariance and the four-fold rotation symmetry around the *z*-axis.

Case	J^{H}	J^{K}	J^{DP}	J^{QP}	A^{SIA}	Ground state	Direction	Degeneracy
1	+	−	−	−	−	AFM	any	SO(3)
2	+	+	−	−	−	AFM	*xy*-plane	Continuous
3	+	−	+	−	−	AFM	*z*	2
4	+	−	−	+	−	AFM	*z*	2
5	+	−	−	−	+	AFM	*z*	2
6	+	+	+	−	−	AFM	*xy*-plane	Continuous
7	+	+	−	+	−	AFM	110	8
8	+	+	−	−	+	AFM	*xy*-plane	Continuous
9	+	−	+	+	−	AFM	*z*	2
10	+	−	+	−	+	AFM	*z*	2
11	+	−	−	+	+	AFM	*z*	2
12	+	+	+	+	−	AFM	110	8
13	+	+	+	−	+	AFM	*xy*-plane	Continuous
14	+	+	−	+	+	AFM	110	8
15	+	−	+	+	+	AFM	*z*	2
16	+	+	+	+	+	AFM	110	8

4. Summary

In summary, we have studied the basal-plane antiferromagnetism in the novel spin–orbit Mott insulator Ba_2IrO_4. We show the basal-plane antiferromagnetism is caused by the intralayer magnetic interactions. We add the SIA and pseudo-quadrupole interaction into the general bilinear pseudo-spin Hamiltonian to unveil the origin of the basal-plane antiferromagnetism. We find that the SIA and pseudo-quadrupole interaction are unexpectedly strong. Based on the systematical MC simulations, we reveal the experimentally observed basal-plane antiferromagnetism can be explained by the isotropic Heisenberg, bond-dependent Kitaev and pseudo-quadrupole interactions. On the basis of this study the SIA and pseudo-quadrupole interactions could play a role in explaining magnetic interactions in other iridates.

Acknowledgments

This paper was partially supported by the National Natural Science Foundation of China, and the Research Program of Shanghai Municipality, the Ministry of Education, and Fok Ying Tung Education Foundation. We are grateful to Dr J H Yang, Y L Zhang for valuable discussions.

Appendix A. The dependence of MAE on the Kitaev, pseudo-dipole and pseudo-quadrupole interactions

In this appendix, we provide some details of the study on the MAE of the bond-dependent Kitaev, pseudo-dipole and pseudo-quadruple interactions. Here we consider an arbitrary AFM(θ, ϕ) state (see the definition in the main text) in the $\sqrt{2} \times \sqrt{2} \times 1$ supercell. For a given Ir–Ir pair denoted as pair *i*, the magnetic moments of this Ir–Ir pair are coupled either antiferromagnetically or ferromagnetically. For example, the magnetic moments of the NN Ir–Ir pair are antiferromagnetically coupled while the magnetic moments of the NNN Ir–Ir pair are ferromagnetically coupled. The polar angle of a given Ir–Ir pair *i* with respect to the *x*-axis is denoted as φ_i. For example, the polar angle φ_{NN} of the NN Ir–Ir pair is $\pi/4$. As a result of the four-fold rotation symmetry around the *z*-axis, there exist other three symmetrically equal Ir–Ir pairs with respect to a given Ir–Ir pair *i*. The polar angles of these four symmetrically equal Ir–Ir pairs are φ_i, $\varphi_i + \pi/2$, $\varphi_i + \pi$ and $\varphi_i + 3\pi/2$, respectively.

The contribution to the MAE from the Kitaev interaction of a given Ir–Ir pair *i* is

$$E_i^{K}(\theta, \phi) = 8C_i J_i^{K} \cos^2\theta. \tag{A.1.0}$$

In equation (A.1.0), J_i^{K} is the Kitaev interaction parameter and C_i is $-1(+1)$ if the given Ir–Ir pair is antiferromagnetically (ferromagnetically) coupled. Especially, the contributions from the NN and NNN Ir–Ir pairs are

$$E_1^{\mathrm{K}}(\theta,\,\phi) = -8J_1^{\mathrm{K}}\cos^2\theta \tag{A.1.1}$$

and

$$E_2^{\mathrm{K}}(\theta,\,\phi) = 8J_2^{\mathrm{K}}\cos^2\theta, \tag{A.1.2}$$

respectively. Summing over all the Ir–Ir pairs farther than the NNN Ir–Ir pairs, we can obtain

$$E^{\mathrm{K}}(\theta,\,\phi) = \sum_i E_i^{\mathrm{K}}(\theta,\,\phi) = \cos^2\theta\sum_i 8C_iJ_i^{\mathrm{K}} = J^{\mathrm{K}}\cos^2\theta. \tag{A.1}$$

As for the contribution from the pseudo-dipole interaction of a given Ir–Ir pair i to the MAE, it is

$$\begin{aligned} E_i^{\mathrm{DP}}(\theta,\,\phi) &= 2C_iJ_i^{\mathrm{DP}}\sin^2\theta\,[\cos^2(\phi-\varphi_i)+\cos^2(\phi-\varphi_i-\pi/2)] \\ &\quad +2C_iJ_i^{\mathrm{DP}}\sin^2\theta\,[\cos^2(\phi-\varphi_i-\pi)+\cos^2(\phi-\varphi_i-3\pi/2)] \\ &= 4C_iJ_i^{\mathrm{DP}}\sin^2\theta. \end{aligned} \tag{A.2.0}$$

Especially, the contributions from the NN and NNN Ir–Ir pairs are

$$E_1^{\mathrm{DP}}(\theta,\,\phi) = -4J_1^{\mathrm{DP}}\sin^2\theta \tag{A.2.1}$$

and

$$E_2^{\mathrm{DP}}(\theta,\,\phi) = 4J_2^{\mathrm{DP}}\sin^2\theta, \tag{A.2.2}$$

respectively. Therefore, the contribution from the pseudo-dipole interaction of the Ir–Ir pairs farther than the NNN Ir–Ir pairs is

$$E^{\mathrm{DP}}(\theta,\,\phi) = \sum_i E_i^{\mathrm{DP}}(\theta,\,\phi) = \sin^2\theta\sum_i 4C_iJ_i^{\mathrm{PD}} = J^{\mathrm{DP}}\sin^2\theta. \tag{A.2}$$

Based on the equations (A.1) and (A.2), we obtain the contribution from the Kitaev and pseudo-dipole interactions of the Ir–Ir pairs farther than the NNN Ir–Ir pairs to the MAE is

$$E(J^{\mathrm{K}},\,J^{\mathrm{DP}},\,\theta,\,\phi) = E^{\mathrm{K}}(\theta,\,\phi) + E^{\mathrm{DP}}(\theta,\,\phi) = J^{\mathrm{K}}\cos^2\theta + J^{\mathrm{DP}}\sin^2\theta. \tag{A.3}$$

Equation (A.3) clears show the MAE is only dependent on the azimuthal angle θ but independent on the polar angle ϕ.

The contribution from the pseudo-quadrupole interaction of the NN Ir–Ir pair to the MAE is

$$\begin{aligned} E_1^{\mathrm{QP}}(\theta,\,\phi) &= 2J_{\mathrm{NN}}^{\mathrm{DP}}\sin^4\theta\,[\cos^4\phi+\cos^4(\phi-\pi/2)+\cos^4(\phi-\pi)+\cos^4(\phi-3\pi/2)] \\ &= 4J_{\mathrm{NN}}^{\mathrm{DP}}\sin^4\theta\,[\cos^4\phi+\sin^4\phi] \\ &= 4J_{\mathrm{NN}}^{\mathrm{DP}}\sin^4\theta\,[1-2\sin^2\phi\cos^2\phi]. \end{aligned} \tag{A.4.1}$$

As for the contribution from the pseudo-quadrupole interaction of the NNN Ir–Ir pair to the MAE, it is

$$\begin{aligned} E_2^{\mathrm{QP}}(\theta,\,\phi) &= 2J_{\mathrm{NNN}}^{\mathrm{DP}}\sin^4\theta\left[\cos^4\left(\phi-\frac{\pi}{4}\right)+\cos^4\left(\phi-\frac{3\pi}{4}\right)+\cos^4\left(\phi-\frac{5\pi}{4}\right)\right. \\ &\quad \left.+\cos^4\left(\phi-\frac{7\pi}{4}\right)\right] \\ &= 4J_{\mathrm{NNN}}^{\mathrm{DP}}\sin^4\theta\,[\cos^4(\phi-\pi/4)+\sin^4(\phi-\pi/4)] \\ &= 4J_{\mathrm{NNN}}^{\mathrm{DP}}\sin^4\theta\,[1-2\sin^2(\phi-\pi/4)\cos^2(\phi-\pi/4)] \\ &= 2J_{\mathrm{NNN}}^{\mathrm{DP}}\sin^4\theta\,[1+4\sin^2\phi\cos^2\phi]. \end{aligned} \tag{A.4.2}$$

Appendix B. SIA of the pseudo-spin state in the tetragonal crystal field

The single ion model Hamiltonian of the Ir^{4+} ion in the cubic crystal field is read as

$$H_{\mathrm{SOC}} = \lambda\boldsymbol{L}\cdot\boldsymbol{S}(\lambda>0). \tag{B.1}$$

Because the energies of e_g orbitals are far above those of the t_{2g} orbitals, H_{SOC} is restricted to the t_{2g} subspace $\{|xz,\uparrow\rangle, |yz,\uparrow\rangle, |xy,\downarrow\rangle, |xz,\downarrow\rangle, |yz,\downarrow\rangle, |xy,\uparrow\rangle\}$ and its matrix presentation is

$$H_{\mathrm{SOC}} = \begin{bmatrix} & xz\uparrow & yz\uparrow & xy\downarrow & xz\downarrow & yz\downarrow & xy\uparrow \\ xz\uparrow & 0 & -\mathrm{i}\frac{\lambda}{2} & \mathrm{i}\frac{\lambda}{2} & 0 & 0 & 0 \\ yz\uparrow & \mathrm{i}\frac{\lambda}{2} & 0 & -\frac{\lambda}{2} & 0 & 0 & 0 \\ xy\downarrow & -\mathrm{i}\frac{\lambda}{2} & -\frac{\lambda}{2} & 0 & 0 & 0 & 0 \\ xz\downarrow & 0 & 0 & 0 & 0 & \mathrm{i}\frac{\lambda}{2} & \mathrm{i}\frac{\lambda}{2} \\ yz\downarrow & 0 & 0 & 0 & -\mathrm{i}\frac{\lambda}{2} & 0 & \frac{\lambda}{2} \\ xy\uparrow & 0 & 0 & 0 & -\mathrm{i}\frac{\lambda}{2} & \frac{\lambda}{2} & 0 \end{bmatrix}.$$

Note that in the t_{2g} subspace the effective total angular momentum operator $\boldsymbol{J}_{\mathrm{eff}}$ is $\boldsymbol{J}_{\mathrm{eff}} = \mathbf{S} - \mathbf{L}$ and the commutation relations are $[J^{\alpha}_{\mathrm{eff}}, \boldsymbol{L}\cdot\boldsymbol{S}] = 0 (\alpha = x, y, z)$ and $[\boldsymbol{J}^2_{\mathrm{eff}}, \boldsymbol{L}\cdot\boldsymbol{S}] = 0$. Therefore J^x_{eff}, J^y_{eff}, J^z_{eff}, and $\boldsymbol{J}_{\mathrm{eff}}$ are all good quantum numbers and the six eigenstates can be labeled as

$$\begin{aligned} |1_{\mathrm{C}}\rangle &= |\boldsymbol{J}_{\mathrm{eff}} = 3/2, J^z_{\mathrm{eff}} = 3/2\rangle, \\ |2_{\mathrm{C}}\rangle &= |\boldsymbol{J}_{\mathrm{eff}} = 3/2, J^z_{\mathrm{eff}} = 1/2\rangle, \\ |3_{\mathrm{C}}\rangle &= |\boldsymbol{J}_{\mathrm{eff}} = 3/2, J^z_{\mathrm{eff}} = -1/2\rangle, \\ |4_{\mathrm{C}}\rangle &= |\boldsymbol{J}_{\mathrm{eff}} = 3/2, J^z_{\mathrm{eff}} = -3/2\rangle, \\ |5_{\mathrm{C}}\rangle &= |\boldsymbol{J}_{\mathrm{eff}} = 1/2, J^z_{\mathrm{eff}} = 1/2\rangle, \\ |6_{\mathrm{C}}\rangle &= |\boldsymbol{J}_{\mathrm{eff}} = 1/2, J^z_{\mathrm{eff}} = -1/2\rangle. \end{aligned}$$

Their corresponding eigenvalues are $-\lambda/2, -\lambda/2, -\lambda/2, -\lambda/2, \lambda$ and λ. Because Ir^{4+} ions have five 5d electrons, the ground state is a single hole residing on the pseudo-spin $|\boldsymbol{J}_{\mathrm{eff}} = 1/2, J^z_{\mathrm{eff}} = 1/2\rangle$ or $|\boldsymbol{J}_{\mathrm{eff}} = 1/2, J^z_{\mathrm{eff}} = -1/2\rangle$ states (Kramers degeneracy). Hereafter, we discuss the pseudo-spin $\boldsymbol{J}_{\mathrm{eff}} = 1/2$ states in the language of holes. Because operators J^x_{eff}, J^y_{eff} and J^z_{eff} commutate with the Hamiltonian H_{SOC}, pseudo-spin $|\boldsymbol{J}_{\mathrm{eff}} = 1/2, J^x_{\mathrm{eff}} = 1/2\rangle$ and $|\boldsymbol{J}_{\mathrm{eff}} = 1/2, J^y_{\mathrm{eff}} = 1/2\rangle$ states are the linear combination of the $|\boldsymbol{J}_{\mathrm{eff}} = 1/2, J^z_{\mathrm{eff}} = 1/2\rangle$ and $|\boldsymbol{J}_{\mathrm{eff}} = 1/2, J^z_{\mathrm{eff}} = -1/2\rangle$ states, namely

$$\begin{aligned} \left|\boldsymbol{J}_{\mathrm{eff}} = \frac{1}{2}, J^x_{\mathrm{eff}} = \frac{1}{2}\right\rangle &= \frac{1}{\sqrt{2}}\left(\left|\boldsymbol{J}_{\mathrm{eff}} = \frac{1}{2}, J^z_{\mathrm{eff}} = \frac{1}{2}\right\rangle + \left|\boldsymbol{J}_{\mathrm{eff}} = \frac{1}{2}, J^z_{\mathrm{eff}} = -\frac{1}{2}\right\rangle\right), \\ \left|\boldsymbol{J}_{\mathrm{eff}} = \frac{1}{2}, J^y_{\mathrm{eff}} = \frac{1}{2}\right\rangle &= \frac{1}{\sqrt{2}}\left(\left|\boldsymbol{J}_{\mathrm{eff}} = \frac{1}{2}, J^z_{\mathrm{eff}} = \frac{1}{2}\right\rangle + \mathrm{i}\left|\boldsymbol{J}_{\mathrm{eff}} = \frac{1}{2}, J^z_{\mathrm{eff}} = -\frac{1}{2}\right\rangle\right). \end{aligned}$$

It can be verified that the energy expectations of the pseudo-spin $|\boldsymbol{J}_{\mathrm{eff}} = 1/2, J^x_{\mathrm{eff}} = 1/2\rangle$, $|\boldsymbol{J}_{\mathrm{eff}} = 1/2, J^y_{\mathrm{eff}} = 1/2\rangle$ and $|\boldsymbol{J}_{\mathrm{eff}} = 1/2, J^z_{\mathrm{eff}} = 1/2\rangle$ states are equal, so the pure pseudo-spin $\boldsymbol{J}_{\mathrm{eff}} = 1/2$ states in the cubic crystal field have no SIA. Therefore the lack of SIA of the pseudo-spin $\boldsymbol{J}_{\mathrm{eff}} = 1/2$ states is protected by the cubic symmetry.

In the tetragonal crystal field, the Hamiltonian is read as

$$\boldsymbol{H} = H_{\mathrm{SOC}} + H_{\Delta} = \lambda \boldsymbol{L}\cdot\boldsymbol{S} + \Delta \times L^2_z. \tag{B.2}$$

In this case, the operators J^x_{eff}, J^y_{eff}, and $\boldsymbol{J}^2_{\mathrm{eff}}$ do not commutate with the Hamiltonian equation (B.2) because of $[J^x_{\mathrm{eff}}, L^2_z] \neq 0$, $[J^y_{\mathrm{eff}}, L^2_z] \neq 0$ and $[\boldsymbol{J}^2_{\mathrm{eff}}, L^2_z] \neq 0$, which indicates that the pseudo-spin $\boldsymbol{J}_{\mathrm{eff}} = 1/2$ states in the tetragonal crystal field are not pure. However, J^z_{eff} commutates with the Hamiltonian equation (B.2) because of $[J^z_{\mathrm{eff}}, L^2_z] = 0$. Therefore J^z_{eff} is still a good quantum number in the presence of the tetragonal crystal field. Furthermore, the expectation $\langle \boldsymbol{J}^2_{\mathrm{eff}}\rangle$ of the operator $\boldsymbol{J}^2_{\mathrm{eff}}$ is close to $\frac{3}{2}\times\left(\frac{3}{2}+1\right)$ and $\frac{1}{2}\times\left(\frac{1}{2}+1\right)$ (see figure B1). So the six eigenstates of the Hamiltonian equation (B.2) can be still labeled by $\boldsymbol{J}^2_{\mathrm{eff}}$ and J^z_{eff}, namely

$$|1_T\rangle = \left| J_{\rm eff} \approx \frac{3}{2}, J^z_{\rm eff} = \frac{3}{2} \right\rangle,$$
$$|2_T\rangle = \left| J_{\rm eff} \approx \frac{3}{2}, J^z_{\rm eff} = \frac{1}{2} \right\rangle,$$
$$|3_T\rangle = \left| J_{\rm eff} \approx \frac{3}{2}, J^z_{\rm eff} = -\frac{1}{2} \right\rangle,$$
$$|4_T\rangle = \left| J_{\rm eff} \approx \frac{3}{2}, J^z_{\rm eff} = -\frac{3}{2} \right\rangle,$$
$$|5_T\rangle = \left| J_{\rm eff} \approx \frac{1}{2}, J^z_{\rm eff} = \frac{1}{2} \right\rangle,$$
$$|6_T\rangle = \left| J_{\rm eff} \approx \frac{1}{2}, J^z_{\rm eff} = -\frac{1}{2} \right\rangle.$$

The ground state is a single hole residing on the pseudo-spin states

$$|5_T\rangle = \left| J_{\rm eff} \approx \frac{1}{2}, J^z_{\rm eff} = \frac{1}{2} \right\rangle = \sin\alpha\ |xy, \uparrow\rangle + \frac{\cos\alpha}{\sqrt{2}}(i\ |xz, \downarrow\rangle + |yz, \downarrow\rangle) \quad \text{(B.3.1)}$$

or

$$|6_T\rangle = \left| J_{\rm eff} \approx \frac{1}{2}, J^z_{\rm eff} = -\frac{1}{2} \right\rangle = \sin\alpha\ |xy, \downarrow\rangle + \frac{\cos\alpha}{\sqrt{2}}(i\ |xz, \uparrow\rangle - |yz, \uparrow\rangle). \quad \text{(B.3.2)}$$

In equations (B.3.1) and (B.3.2) the angle α parameterizes the relative strength of the tetragonal crystal-field splitting and $\tan(2\alpha) = 2\sqrt{2}\,\lambda/(\lambda - \Delta)$ (Δ is the tetragonal crystal-field splitting). Because the operator $J^x_{\rm eff}$ does not commutate with the Hamiltonian equation (B.2), the pseudo-spin $|J_{\rm eff} \approx 1/2, J^x_{\rm eff} = 1/2\rangle$ state is not a linear combination of the $|J_{\rm eff} \approx 1/2, J^z_{\rm eff} = 1/2\rangle$ and $|J_{\rm eff} \approx 1/2, J^z_{\rm eff} = -1/2\rangle$ states. Actually, the desired pseudo-spin $|J_{\rm eff} \approx 1/2, J^x_{\rm eff} = 1/2\rangle$ state is a linear combination of the $J_{\rm eff} \approx 3/2$ and pseudo-spin $J_{\rm eff} \approx 1/2$ states, that is

$$\left| J_{\rm eff} \approx \frac{1}{2}, J^x_{\rm eff} = \frac{1}{2} \right\rangle = C_1\ |1_T\rangle + C_2\ |2_T\rangle + C_3\ |3_T\rangle + C_4\ |4_T\rangle + C_5\ |5_T\rangle + C_6\ |6_T\rangle. \quad \text{(B.4)}$$

In equation (B.4) the coefficients $C_i (i = 1, 2, 3, 4, 5, 6)$ should satisfy such constraints:

$$C_1^\dagger C_1 + C_2^\dagger C_2 + C_3^\dagger C_3 + C_4^\dagger C_4 + C_5^\dagger C_5 + C_6^\dagger C_6 = 1,$$
$$\left\langle J_{\rm eff} \approx \frac{1}{2}, J^x_{\rm eff} = \frac{1}{2} \right| J^x_{\rm eff} \left| J_{\rm eff} \approx \frac{1}{2}, J^x_{\rm eff} = \frac{1}{2} \right\rangle = \frac{1}{2},$$
$$\left\langle J_{\rm eff} \approx \frac{1}{2}, J^x_{\rm eff} = \frac{1}{2} \right| J^2_{\rm eff} \left| J_{\rm eff} \approx \frac{1}{2}, J^x_{\rm eff} = \frac{1}{2} \right\rangle = \left\langle J_{\rm eff} \approx \frac{1}{2}, J^z_{\rm eff} = \frac{1}{2} \right| J^2_{\rm eff} \left| J_{\rm eff} \approx \frac{1}{2}, J^z_{\rm eff} = \frac{1}{2} \right\rangle.$$

So it is natural to expect that the energy expectation of the $|J_{\rm eff} \approx 1/2, J^x_{\rm eff} = 1/2\rangle$ state is different from that of the $|J_{\rm eff} \approx 1/2, J^z_{\rm eff} = 1/2\rangle$ state. Whatever the tetragonal crystal field splitting Δ is, the ground state of the Ir^{4+} ion is a single hole residing on the pseudo-spin $|J_{\rm eff} \approx 1/2, J^z_{\rm eff} = 1/2\rangle$ state. For the sake of producing the desired pseudo-spin $|J_{\rm eff} \approx 1/2, J^x_{\rm eff} = 1/2\rangle$ state, the single hole should have the possibility of residing on the lower-energy $|J_{\rm eff} \approx 3/2\rangle$ state. For the hole, the lower-energy state is not favored. So the z-axis is the easy axis of the pseudo-spin state of the Ir^{4+} ion in the tetragonal crystal field, which is consistent our DFT calculated results. Therefore it is the symmetry lowering from the cubic to the tetragonal that makes the pseudo-spin state have the SIA.

We introduce a new Hamiltonian $\boldsymbol{H}^{\rm new}$ by adding a constraint term $\boldsymbol{\alpha} \cdot \boldsymbol{J}_{\rm eff}$ onto the Hamiltonian equation (B.2) so as to confirm the above results numerically:

$$\boldsymbol{H}^{\rm new} = H_{\rm SOC} + H_\Delta + H_{\rm constraint} = \lambda \boldsymbol{L} \cdot S + \Delta \times L_z^2 + \boldsymbol{\alpha} \cdot \boldsymbol{J}_{\rm eff}. \quad \text{(B.5)}$$

The constraint term is merely used to construct the desirable state. In equation (B.5), the parameter $\boldsymbol{\alpha}$ is a real vector and in the form of $\boldsymbol{\alpha} = (\alpha_x, \alpha_y, \alpha_z)$. If the parameter $\boldsymbol{\alpha}$ is set to be $\boldsymbol{\alpha} = (\alpha_x, 0, 0)$ $(\alpha_x > 0)$, the equation (B.5) will select out a specific hole state $|J_x\rangle$ which approaches to the pseudo-spin $|J_{\rm eff} \approx 1/2, J^x_{\rm eff} = 1/2\rangle$ state. Likewise, the equation (B.5) will select out a specific hole state $|J_z\rangle$ which approaches to the pseudo-spin $|J_{\rm eff} \approx 1/2, J^z_{\rm eff} = 1/2\rangle$ state if the parameter $\boldsymbol{\alpha}$ is set to be $\boldsymbol{\alpha} = (0, 0, \alpha_z)$ $(\alpha_z > 0)$. For the selected hole states $|J_x\rangle$ and $|J_z\rangle$, their energy expectation are calculated based on the formulas $E(J_x) = \langle J_x|\ H_{\rm SOC} + H_\Delta\ |J_x\rangle$ and $E(J_z) = \langle J_z|\ H_{\rm SOC} + H_\Delta\ |J_z\rangle$ such that the effect of the constraint is removed. Note that the denotation $E(J_z = 1/2)$ in the figure B2 is the energy of the hole eigenstate $|J_{\rm eff} \approx 1/2, J^z_{\rm eff} = 1/2\rangle$ of the equation (B.2). Because the operator $J^z_{\rm eff}$ still commutates with the Hamiltonian equation (B.5) in the case of $\boldsymbol{\alpha} = (0,0, \alpha_z)$, the selected hole state $|J_z\rangle$ is the hole eigenstate $|J_{\rm eff} \approx 1/2, J^z_{\rm eff} = 1/2\rangle$ of the equation (B.2), which is consistent with the vanishing energy difference $\Delta E_Z = E(J_z) - E(J_z = 1/2)$ and the constant

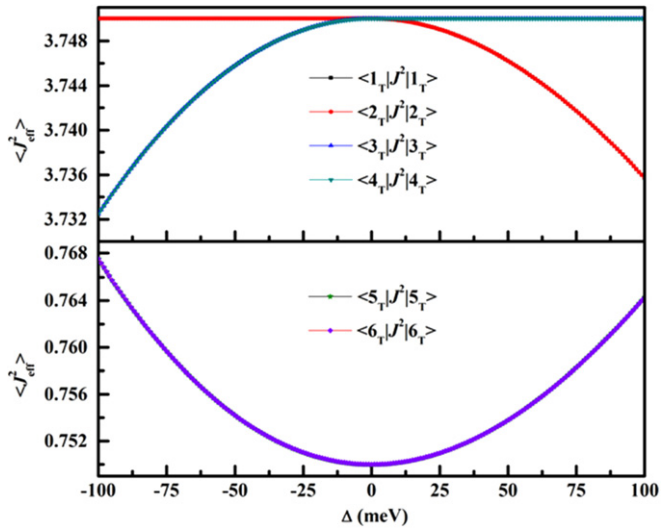

Figure B1. Expectation $\langle J^2_{\rm eff}\rangle$ of the six eigenstates labeled by $|i_{\rm T}>$ ($i = 1,\ 2,\ 3,\ 4,\ 5,\ 6$) of the Hamiltonian equation (B.2).

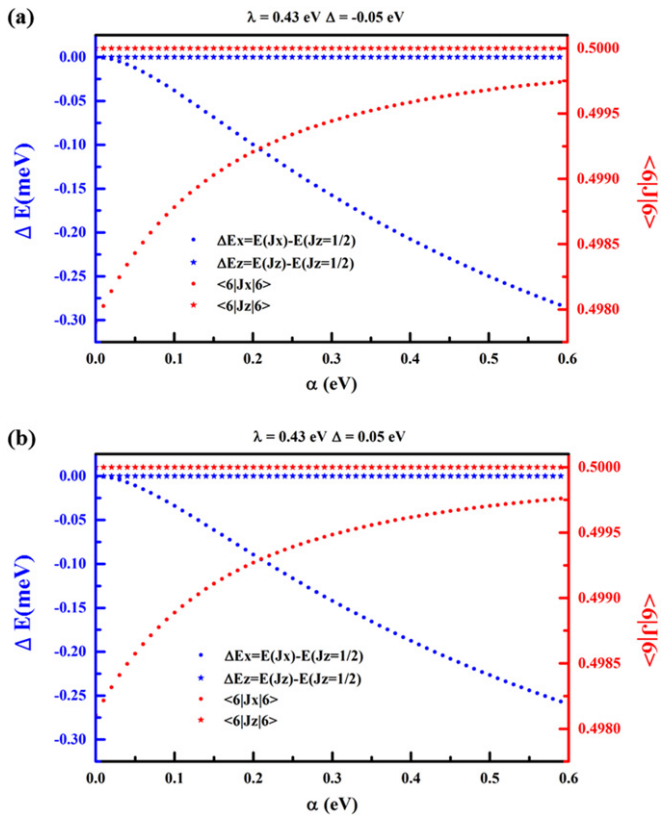

Figure B2. The dependence on the constraint parameter α of the expectation $\langle J_x\rangle$ (read circle), $\langle J_z\rangle$ (read star) and energy difference $\Delta Ex = E(J_x)$-$E(J_z = 1/2)$ (blue circle), $\Delta Ez = E(J_z)$-$E(J_z = 1/2)$ (blue star) of the selected hole states based on the Hamiltonian equation (B.5) in the tetragonal crystal field splitting $\Delta < 0$ (a) and $\Delta > 0$ (b). The selected hole state is denoted by $|6\rangle$. Here we set the tetragonal crystal field splitting Δ to be 50 meV according to the [32].

$\langle J_z\rangle = 0.5$ (see the figure B2). It is clearly shown in the figure B2 that the selected holes state $|J_x\rangle$ has a higher energy than the hole eigenstate $|\boldsymbol{J}_{\rm eff} \approx 1/2,\ J^z_{\rm eff} = 1/2\rangle$ no matter the tetragonal distortion is elongation ($\Delta > 0$) or compression ($\Delta < 0$) along the z-axis, which indicates that the easy axis is the z-axis. Therefore the pseudo-spin $\boldsymbol{J}_{\rm eff} \approx 1/2$ state in Ba_2IrO_4 with the tetragonal symmetry has SIA and its easy axis is the z-axis, which is consistent with our DFT calculated results.

We would like to emphasize the appearance of the SIA in the pseudo-spin state of Ir^{5+} ions in the tetragonal crystal field does not contradict with the consensus that absence of SIA applies to any two-level system with Kramers degeneracy, which is because of the following two important factors. Firstly, our DFT calculations indicate that pseudo-spin state in Ba_2IrO_4 is not the ideal $J_{\rm eff} = 1/2$ state which is a two-level system with Kramers degeneracy, because its magnetic moments is about 0.5 μB (0.32 μB from orbit and 0.18 μB from spin) which deviates from the expected 1.0 μB (0.67 μB from orbit and 0.33 μB from spin) of the ideal $J_{\rm eff} = 1/2$ state. Secondly, as discussed above, the tetragonal crystal field splitting (Δ) in Ba_2IrO_4 can mix the pseudo-spin state with non-pure $J_{\rm eff} \approx 3/2$ states. So the pseudo-spin state in Ba_2IrO_4 is not an exact two-level system because non-pure $J_{\rm eff} \approx 3/2$ states are involved. Taking non-pure $J_{\rm eff} \approx 3/2$ states into account, we propose that the pseudo-spin state in Ba_2IrO_4 is a six-level non-degenerate system at least. So it is possible to have SIA.

Appendix C. Calculations of interaction parameters in model Hamiltonian

Here we take the NN Ir–Ir pairs as an example to demonstrate how interaction parameters in the finial model Hamiltonian (see equation (10) in the main text) are figured out based the DFT + U + SOC calculations. By setting the x- and y-axes along NN Ir–Ir pairs and z-axis orthogonal to the IrO_2 layer, we can rewrite the finial model Hamiltonian into the new one:

$$H = \sum_{\langle i,j\rangle \in xy} [H_{\langle i,j\rangle \|x} + H_{\langle i,j\rangle \|y} + J_{ij}^{\rm QP}(\bar{\boldsymbol{S}}_i \cdot \boldsymbol{r}_{ij})^2(\boldsymbol{r}_{ij} \cdot \bar{\boldsymbol{S}}_j)^2] + \sum_i A_i^{\rm SIA}(\bar{S}_i^z)^2$$
$$\sum_{\langle\langle i,j\rangle\rangle \in xy} [J_{ij}^{\rm H}\bar{\boldsymbol{S}}_i \cdot \bar{\boldsymbol{S}}_j + J_{ij}^{\rm K}\bar{S}_i^z\bar{S}_j^z + J_{ij}^{\rm DP}(\bar{\boldsymbol{S}}_i \cdot \boldsymbol{r}_{ij})(\boldsymbol{r}_{ij} \cdot \bar{\boldsymbol{S}}_j) + J_{ij}^{\rm QP}(\bar{\boldsymbol{S}}_i \cdot \boldsymbol{r}_{ij})^2(\boldsymbol{r}_{ij} \cdot \bar{\boldsymbol{S}}_j)^2]. \quad \text{(C.1)}$$

The two-site effective spin Hamiltonians $H_{\langle i,j\rangle \|x}$ and $H_{\langle i,j\rangle \|y}$ for NN Ir–Ir pairs along the x- and y-axis can then be written as

$$H_{\langle i,j\rangle \|x} = J_{ij}^{\|} S_i^x S_j^x + J_{ij}^{\rm H} S_i^y S_j^y + J_{ij}^{\perp} S_i^z S_j^z, \quad \text{(C.2)}$$

$$H_{\langle i,j\rangle \|y} = J_{ij}^{\rm H} S_i^x S_j^x + J_{ij}^{\|} S_i^y S_j^y + J_{ij}^{\perp} S_i^z S_j^z, \quad \text{(C.3)}$$

$$J_{ij}^{\|} = J_{ij}^{\rm H} + J_{ij}^{\rm DP}, \quad \text{(C.4)}$$

$$J_{ij}^{\perp} = J_{ij}^{\rm H} + J_{ij}^{\rm K}. \quad \text{(C.5)}$$

Using the four-state mapping method [45] and by setting magnetic moments along the x-, y- and z-axes, respectively, we can figure out the $J_{ij}^{\|}$, $J_{ij}^{\rm H}$ and $J_{ij}^{\perp}$ for a NN Ir–Ir pair along the x-axis, for example. According to the equations (C.4) and (C.5), we can figure out the Heisenberg interaction parameter $J_{ij}^{\rm H}$, pseudo-dipole interaction parameter $J_{ij}^{\rm DP}$ and bond-dependent Kitaev interaction parameter $J_{ij}^{\rm K}$. Similarly, we can figure out these parameters by setting the x- and y-axes along NNN Ir–Ir pairs and z-axis orthogonal to the IrO_2 layer. As for the NN and NNN pseudo-quadrupole interaction parameters $J_1^{\rm QP}$, $J_2^{\rm QP}$ and SIA parameters $A^{\rm SIA}$, they can calculated based on the MAE coefficients equations (9.1)–(9.3).

References

[1] Kim B J, Ohsumi H, Komesu T, Sakai S, Morita T, Takagi H and Arima T 2009 *Science* **323** 1329
[2] Kim B J *et al* 2008 *Phys. Rev. Lett.* **101** 076402
[3] Shitade A, Katsura H, Kunes J, Qi X L, Zhang S C and Nagaosa N 2009 *Phys. Rev. Lett.* **102** 256403
[4] Singh Y, Manni S, Reuther J, Berlijn T, Thomale R, Ku W, Trebst S and Gegenwart P 2012 *Phys. Rev. Lett.* **108** 127203
[5] Pesin D and Balents L 2010 *Nat. Phys.* **6** 376
[6] Yang B-J and Kim Y B 2010 *Phys. Rev.* B **82** 085111
[7] Wan X, Turner A M, Vishwanath A and Savrasov S Y 2011 *Phys. Rev.* B **83** 205101
[8] Jackeli G and Khaliullin G 2009 *Phys. Rev. Lett.* **102** 017205
[9] Chaloupka J, Jackeli G and Khaliullin G 2010 *Phys. Rev. Lett.* **105** 027204
[10] Reuther J, Thomale R and Trebst S 2011 *Phys. Rev.* B **84** 100406
[11] Kitaev A 2006 *Ann. Phys., NY* **321** 2
[12] Wang F and Senthil T 2011 *Phys. Rev. Lett.* **106** 136402
[13] Watanabe H, Shirakawa T and Yunoki S 2013 *Phys. Rev. Lett.* **110** 027002
[14] Kim J *et al* 2012 *Phys. Rev. Lett.* **108** 177003
[15] Kim Y K, Krupin O, Denlinger J D, Bostwick A, Rotenberg E, Zhao Q, Mitchell J F, Allen J W and Kim B J 2014 *Science* **345** 187
[16] Crawford M K, Subramanian M A, Harlow R L, Fernandezbaca J A, Wang Z R and Johnston D C 1994 *Phys. Rev.* B **49** 9198
[17] Cao G, Bolivar J, McCall S, Crow J E and Guertin R P 1998 *Phys. Rev.* B **57** 11039
[18] Okabe H *et al* 2011 *Phys. Rev.* B **83** 155118
[19] Okabe H, Isobe M, Takayama-Muromachi E, Takeshita N and Akimitsu J 2013 *Phys. Rev.* B **88** 075137
[20] Boseggia S *et al* 2013 *Phys. Rev. Lett.* **110** 117207
[21] Moser S *et al* 2014 *New J. Phys.* **16** 013008
[22] Katukuri V M, Yushankhai V, Siurakshina L, van den Brink J, Hozoi L and Rousochatzakis I 2014 *Phys. Rev.* X **4** 021051

[23] Perdew J P, Burke K and Ernzerhof M 1996 *Phys. Rev. Lett.* **77** 3865
[24] Blöchl P E 1994 *Phys. Rev.* B **50** 17953
[25] Liechtenstein A I, Anisimov V I and Zaanen J 1995 *Phys. Rev.* B **52** R5467
[26] Arita R, Kunes J, Kozhevnikov A V, Eguiluz A G and Imada M 2012 *Phys. Rev. Lett.* **108** 086403
[27] Zhang H, Haule K and Vanderbilt D 2013 *Phys. Rev. Lett.* **111** 246402
[28] Liu X *et al* 2012 *Phys. Rev. Lett.* **109** 157401
[29] Sala M M, Boseggia S, McMorrow D F and Monaco G 2014 *Phys. Rev. Lett.* **112** 026403
[30] Hukushima K and Nemoto K 1996 *J. Phys. Soc. Japan* **65** 1604
[31] Wang P S, Ren W, Bellaiche L and Xiang H J 2015 *Phys. Rev. Lett.* **114** 147204
[32] Sala M M *et al* 2014 *Phys. Rev.* B **89** 121101
[33] Mason W P 1954 *Phys. Rev.* **96** 302
[34] Escudier P 1975 *Ann. Phys., Paris* **9** 125
[35] Jin H, Jeong H, Ozaki T and Yu J 2009 *Phys. Rev.* B **80** 075112
[36] Perkins N B, Sizyuk Y and Woelfle P 2014 *Phys. Rev.* B **89** 035143
[37] Moriya T and Yosida K 1953 *Prog. Theor. Phys.* **9** 663
[38] Liu J, Koo H-J, Xiang H, Kremer R K and Whangbo M-H 2014 *J. Chem. Phys.* **141** 124113
[39] Xiang H J, Kan E J, Whangbo M H, Lee C, Wei S-H and Gong X G 2011 *Phys. Rev.* B **83** 174402
[40] Foyevtsova K, Jeschke H O, Mazin I I, Khomskii D I and Valenti R 2013 *Phys. Rev.* B **88** 035107
[41] Liu P, Khmelevskyi S, Kim B, Marsman M, Li D, Chen X-Q, Sarma D D, Kresse G and Franchini C 2015 *Phys. Rev.* B **92** 054428
[42] Van Vleck J H 1937 *Phys. Rev.* **52** 1178
[43] Katukuri V M, Stoll H, van den Brink J and Hozoi L 2012 *Phys. Rev.* B **85** 220402
[44] Katukuri V M *et al* 2014 *New J. Phys.* **16** 013056
[45] Xiang H, Lee C, Koo H-J, Gong X and Whangbo M-H 2013 *Dalton Trans.* **42** 823